Separation Science and Technology
Publication details, including instructions for authors and subscription information:
http://www.informaworld.com/smpp/title~content=t713708471

Numerical Simulation of Continuous Stirred Ultrafiltration Process: An Approach Based on Moving Boundary Layer Concept

Chiranjib Bhattacharjee[a]; Siddhartha Datta[a]
[a] Department of Chemical Engineering, Jadavpur University, Calcutta, India

Online publication date: 04 July 2003

To cite this Article Bhattacharjee, Chiranjib and Datta, Siddhartha(2003) 'Numerical Simulation of Continuous Stirred Ultrafiltration Process: An Approach Based on Moving Boundary Layer Concept', Separation Science and Technology, 38: 8, 1749 — 1772
To link to this Article: DOI: 10.1081/SS-120019407
URL: http://dx.doi.org/10.1081/SS-120019407

MARCEL DEKKER, INC. • 270 MADISON AVENUE • NEW YORK, NY 10016

SEPARATION SCIENCE AND TECHNOLOGY
Vol. 38, No. 8, pp. 1749–1772, 2003

Numerical Simulation of Continuous Stirred Ultrafiltration Process: An Approach Based on Moving Boundary Layer Concept

Chiranjib Bhattacharjee* and Siddhartha Datta

Department of Chemical Engineering, Jadavpur University, Calcutta, India

ABSTRACT

A mass transfer model based on unsteady state mass balance over concentration boundary layer coupled with gradual development of so called "gel" or "cake" layer has been formulated in this study. The model considers the boundary layer problem simultaneously with the film theory of mass transfer and resistance in series model. The resulting equations are solved first by reducing the set of partial differential equations to nonlinear equations utilizing orthogonal collocation technique and then applying multidimensional Newton–Raphson method with suitable seeding scheme to solve the above-mentioned nonlinear equations together with some additional constraints. The problem of determination of membrane surface concentration is eliminated by this simultaneous solution of boundary layer equation together with gel layer.

*Correspondence: Professor Chiranjib Bhattacharjee, Dept. of Chemical Engineering, Jadavpur University, Calcutta-700032, India; Fax: +91 33 414 6378; E-mail: c_bhatta@hotmail.com.

DOI: 10.1081/SS-120019407 0149-6395 (Print); 1520-5754 (Online)

MARCEL DEKKER, INC. • 270 MADISON AVENUE • NEW YORK, NY 10016

The model is found to be capable of predicting permeate flux and rejection under different experimental conditions. The main feature of this model is that it takes into account realistically the effect of gel layer formation within concentration boundary layer whereas in most of the previous studies this effect has not been considered. The dependency of concentration profile, gel thickness, and permeate concentration with different operating variables are also studied and the variations are found to be quite reasonable.

Key Words: Ultrafiltration; Boundary layer; Mass transfer; Numerical modeling; Rejection.

INTRODUCTION

Over the past few decades, ultrafiltration (UF), which is a pressure driven membrane process, has emerged as a viable process for the concentration or separation of moderate to high molecular weight solutes from its solutions. The major problem in the commercial use of ultrafiltration is the flux decline with time. As a result of this deleterious effect upon permeate flux, there have been many investigations regarding the nature of transport phenomena in UF, particularly in the vicinity of the membrane surface. Some researcher, point out that the reduction of permeate flux may have originated from the variation of viscosity due to the concentration polarization, independent of any supposed gelation or osmotic effect.[1,2] Several models were developed so far to describe the polarization phenomena in ultrafiltration. Usually all of them can be classified into the following three categories: (a) resistance in series model, (b) gel polarization model, and (c) osmotic pressure model. According to the gel polarization model,[3] a gel layer is formed on the membrane surface. As shown by Wijmans, Nakao, and Smolders,[4] the three models mentioned above predict almost equivalent permeate fluxes under a steady-state condition, especially at higher concentrations. On the other hand, it was shown by Danes, Boriou, and Poyen[5] that no classical model as stated above could explain the experimental data with good fit. Due to this reason, most of the models that are reported in literature are composite in nature, not based directly on any classical models as listed above.

The gel polarization model was well discussed by Nakao, Yumoto, and Kimura.[6] The rejection characteristics of the macromolecular solutes in the low to moderate molecular weight range have been discussed in this paper for the gel-limited case of ultrafiltration. Recently, computer simulation was

discussed by Lebrun et al.[7] to calculate membrane performance data for rectangular slit configuration. This has been achieved by coupling the surface force–pore flow model for membrane transport and concentration polarization model through a boundary condition. Recently very good work in formulating the concentration polarization phenomena has been reported by Song and Elimelech.[8] Their model applies to concentration polarization of noninteracting particles in cross flow filtration system. The theory reveals that a dimensionless number, called filtration number, characterizes the extent of concentration polarization. Effects of natural convection instability on membrane performance in dead-end cross flow ultrafiltration were discussed recently in an interesting manner by Youm, Fane, and Wiley.[9] A mass transfer correlation for mixed convection membrane system was also presented. A significant work regarding modeling of concentration polarization and depolarization with high frequency back pulsing was reported by Redkar, Kuberkar, and Davis.[10] Presently a unified model for predictions of flux in stirred and unstirred batch ultrafiltration was also reported.[11] An integrated model taking into account the gel layer, osmotic pressure and resistance-in-series models has been developed recently by de Pinho, Semiao and Geraldes.[12] This model was formulated for nanofiltration, though it is suggested that it can be extended to reverse osmosis and ultrafiltration. Very recently, a two-dimensional composite model has been discussed by Paris, Guichardon, and Charbit[13] and, comparison of this model with classical models has been performed. It was shown that the developed model is much more superior compared with classical ones.

So far various works have been reported on the analysis of limiting flux phenomena in ultrafiltration. Some works were oriented towards prediction of permeate flux based on some parameters and operating conditions.[14,15] However, very little attention has been paid to the prediction of rejection during ultrafiltration of macromolecular solutes. Neimi, Raimoaho, and Palosaari[16] developed a model for the prediction of both flux and rejection during ultrafiltration. The model was, in fact, based on the finely porous model that described permeate flux and rejection in terms of four quantities.

The present work has been undertaken in an attempt to develop a composite mathematical model that is capable of predicting rejection and flux as well as permits the analysis of dynamic behavior of the deposited gel layer and concentration profile within the boundary layer. The present model is based on a feature that is generally neglected in most of the previous analyses. The concentration-polarization boundary-layer thickness is usually assumed to depend on the shear rate or stirring rate, and to not change as the gel layer grows. In the present model, however, the polarization layer is assumed to become thinner as the gel layer becomes thicker, presumably because

the effects of stirring become greater. So this model is based on a new hypothesis that the total thickness comprising of "effective boundary layer" and deposited solute layer remains constant at a value suggested by film theory of mass transfer. The deposited solute layer grows in thickness with time due to more and more rejection of the solutes by the membrane. Since the total thickness is assumed to be constant, this deposited solute layer, in fact, reduces the thickness of "effective boundary layer", where the concentration gradient actually lies. No such studies in this respect have been made before, and therefore this model would help in analyzing the mass transfer characteristics of solutes during UF under various hydrodynamic conditions, particularly in the vicinity of the membrane.

THEORY

Figure 1 shows the gel layer and concentration boundary layer along with different notations. According to the assumption of this study, the growing thickness of gel layer actually reduces the effective boundary layer and as a result the concentration gradient constantly increases with time until the development of steady state. In all of the previous studies, it has been assumed that the thickness of the concentration boundary layer does not change with time, whereas gel-type layer gradually grows in thickness between

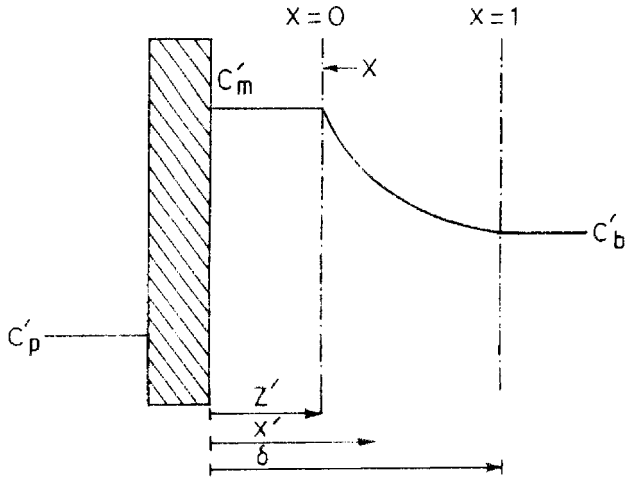

Figure 1. Effective boundary layer and gel formation over the membrane.

the membrane and boundary layer. This means that the boundary layer just shifts away from the membrane to accommodate the growing gel layer. But in the case of continuous stirred ultrafiltration, this seems to be somewhat improbable because of the presence of turbulence created by stirring. So the effect of stirring does not allow any concentration gradient to exist at a distance far away from the membrane. This fact was not considered in any one of the previous studies; instead it was assumed that the boundary layer gradually moves away from the membrane surface, though its thickness and concentration gradient do not change. But in the present study it has been assumed that the flux decline occurs due to the effect of increasing thickness of gel layer, as well as due to increased concentration gradient in the effective boundary layer which in turn increases the back diffusive flux.

The unsteady state mass balance in the effective boundary layer gives the following partial differential equation:

$$\frac{\partial c'}{\partial t'} = J\frac{\partial c'}{\partial x'} + D\frac{\partial^2 c'}{\partial x'^2} \tag{1}$$

The above equation assumes constant diffusivity and density. The initial and boundary conditions, which are applicable to the above equation, are as follows:

i) At $t' = 0$, $c' = c'_b$ for all x'

ii) At $x' = z'$ (which is itself a function of time),

$$c' = c'_m \text{ (an unknown quantity) for } t' > 0$$

iii) At $x' = \delta$, $c' = c'_b$ for $t' \geq 0$ (2)

Introducing the dimensionless variables in the following form

$$c = c'/c'_b, \quad x = (x' - z')/(\delta - z'), \quad t = Dt'/\delta^2 \text{ and } z = z'/\delta \tag{3}$$

(above change in space co-ordinate brings the limit of integration to [0,1], which is independent of time), Eqs. (1) and (2) become:

$$\frac{\partial c}{\partial t} = \frac{1}{(1-z)^2}\left[\frac{J(t)}{k}\frac{\partial c}{\partial x} + \frac{\partial^2 c}{\partial x^2}\right] \tag{4}$$

with the boundary condition represented in the dimensionless form:

i) At $t = 0$, $c = 1$ for all x

ii) At $x = 0$, $c = c_m$ (still unknown) for $t > 0$

iii) At $x = 1$, $c = 1$ for $t \geq 0$ (5)

According to film theory, mass transfer coefficient (k) can be equated to (D/δ), where δ be the film thickness. Since the total thickness (δ) comprising the gel layer and the effective boundary layer remains constant as per the propositions made in this study, the effective boundary (film) layer whose thickness is $\delta - z'$, must shrink to accommodate for the increasing thickness of the gel layer (z). So the mass transfer coefficient should be related according to the equation: $k = D/(\delta - z')$, which in dimensionless form becomes: $D/\delta = k(1 - z)$ and this has been incorporated to get the final form of Eq. (4). With increase in t, mass transfer coefficient should increase according to the above proposition (since, as $1 - z$ decreases, k should increase to keep D/δ constant), which in fact seems reasonable due to increased concentration gradient. For a stirred cell, the mass transfer coefficient at a fixed hydrodynamic condition can be found from well-known empirical correlation[17]:

$$k = 0.0443\,(D/r)(\nu/D)^{0.33}(\omega r^2/\nu)^{0.8} \tag{6}$$

It is a well-established fact that boundary layer develops almost instantaneously, thickness of which will remain constant as a function of time, as postulated in this model. Mass transfer coefficient for calculation of this film thickness (δ) was calculated from Eq. (6) at the given hydrodynamic condition and at the physical properties (viscosity and density) value evaluated at bulk concentration. Further, the diffusivity can be empirically related to molecular weight of polymer solution[18]:

$$D = 2.74 \times 10^{-9} M^{-1/3} \tag{7}$$

Now Eqs. (4) and (5) can be expressed in terms of orthogonal collocation (OC) expression. Using n-point OC with Legendre polynomial [defined for interval (0,1), being the collocation function] Eq. (4) can be expressed for i-th internal

point as follows[19]:

$$\frac{dc_i}{dt} = \frac{1}{[1 - z(t)]^2}\left[\frac{J(t)}{k}\sum_{j=1}^{n+2} A_{ij}c_j + \sum_{j=1}^{n+2} B_{ij}c_j\right] \tag{8}$$

for $i = 2, 3, \ldots, n + 1$.

Here the interval in the effective boundary layer has been divided into $(n + 1)$ subintervals with n internal points $(2, 3, \ldots, n + 1)$ and two boundary points (1 and $n + 2$). The total n number of equations represented by Eq. (8) involves $n + 4$ number of unknowns (namely, $c_1, c_2, \ldots, c_{n+1}, z, J,$ and c_p). So, additional four equations are required to solve the problem.

Unsteady state mass balance over the deposited "gel" or "cake" layer gives the following equation:

$$Jc'|_{x'=z'} - Jc'_p + D\left.\frac{\partial c'}{\partial x'}\right|_{x'=z'} = \frac{\partial z'}{\partial t'}c'$$

or, in terms of dimensionless quantities as defined earlier and after breaking the derivative term with n-point OC, one can get,

$$\frac{dz}{dt} = \left[Jc_1 - Jc_p + k\sum_{j=1}^{n+2} A_{1j}c_j\right]\frac{1}{kc_1(1 - z)} \tag{9}$$

In this study, it is assumed that the total amount of solute in effective boundary layer does not change with time. The solute accumulates only in the "cake" or "gel" layer. During ultrafiltration process, out of the total solute rejected by the membrane, one part gets dissolved in the bulk due to back diffusion and the remaining gets accumulated in the gel layer. Since the solute content of the effective boundary layer does not change, one can write,

$$\frac{d}{dt'}[(\delta - z')\bar{c}'] = 0 \tag{10}$$

where $\bar{c}'$ is the average concentration in the effective boundary layer, which may be a function of time. Using Gauss–Legendre quadrature [defined for interval (0,1)] the above equation can be written as follows[19]:

$$(1 - z)\sum_{j=2}^{n+1} w_j\frac{dc_j}{dt} = \frac{dz}{dt}\sum_{j=2}^{n+1} w_j c_j \tag{11}$$

where w_j are weightage factor for n-point Gauss–Legendre quadrature formula for the interval (0,1). All the values are tabulated and obtained from elsewhere.[19] In the above equation, summation should be over the entire

interval, i.e., from 1 to n + 2. But for all n, except n = 1, which has not been used here due to poor accuracy and instability inherent in 1-point OC; $w_1 = w_{n+2} = 0$.[19]

From this point onwards, computations can be performed in two directions—one is for analysis purpose where experimental values of flux (J) and permeate concentration (c_p) have been used as a function of time and other for prediction purpose, where J and c_p were also predicted along with all other variables. For the first part, Eqs. (8), (9), and (11) can be simultaneously solved for n + 2 number of unknowns ($c_1, c_2, \ldots, c_{n+2}, z$). The two methods produce very small differences in the final computed values of different concentrations and gel thickness. In fact, the latter method is preferred because it predicts J and c_p along with the calculation of the above-mentioned n + 2 variables. Another two equations or conditions are necessary for this purpose. Permeate flux can be expressed by filtration theory in the following form (coupled with osmotic pressure model):

$$J(t) = \frac{\Delta P - \sigma \Delta \pi}{(R_m + \alpha c_1' z')\mu_s} \quad \text{or in terms of dimensionless quantities as introduced earlier,}$$

$$J(t) = (\Delta P - \sigma \Delta \pi)\left[R_m \mu_s + \alpha c_1 c_b' \mu_s \frac{zD}{k(1-z)}\right]^{-1} \tag{12}$$

Osmotic pressure of polymer solution was calculated from well-known Flory's equation.[20] The results from irreversible thermodynamics[21] show that the "real" rejection is related to flux and permeability of the membrane by the following expression:

$$1 - \frac{c_p}{c_1} = \frac{\sigma(1-F)}{1-\sigma F} \quad \text{where} \quad F = \exp[-(1-\sigma)J/P_m] \tag{13}$$

Now all the above n + 4 equations represented by Eqs. (8), (9), (11), (12), and (13) can be solved simultaneously for n + 4 variables. The orthogonal collocation method when applied to parabolic partial differential equation often produces a "stiff" set of ordinary differential equations. Due to this reason, a second order implicit method e.g., the Crank Nicholson method, which has very strong stability envelop, has been used. In fact it is an "A–Stable" technique. Introducing new

variables for the unknowns: $y_i = c_i, (i = 1, \ldots, n+1), y_{n+2} = z, y_{n+3} = J$ and $y_{n+4} = c_p$, the different equations can be written as follows:

i) The set of equation defined by Eq. (8) can be expressed as follows:

$$\frac{dy_{i+1}}{dt} = \Im_i(\underline{y}) \quad \Rightarrow y_{i+1}^{(k+1)} = y_{i+1}^{(k)} + \frac{\Delta t}{2}\left[\Im_i^{(k)} + \Im_i^{(k+1)}\right] \tag{14}$$

where

$$\Im_i(\underline{y}) = \frac{1}{\left[1 - y_{n+2}\right]^2} \times \left[\frac{y_{n+3}}{k}\sum_{j=1}^{n+1} A_{ij}y_j + \sum_{j=1}^{n+1} B_{ij}y_j + \frac{y_{n+3}}{k}A_{i,n+2} + B_{i,n+2}\right]$$

for i = 1, 2, 3, . . ., n.

ii) The Eq. (9) can similarly be represented as:

$$\frac{dy_{n+2}}{dt} = \Im_{n+1}(\underline{y}) \quad \Rightarrow y_{n+2}^{(k+1)} = y_{n+2}^{(k)} + \frac{\Delta t}{2}[\Im_{n+1}^{(k)} + \Im_{n+1}^{(k+1)}] \tag{15}$$

$$\text{where } \Im_{n+1} = \left[Jy_1 - Jy_{n+4} + k\sum_{j=1}^{n+1} A_{1j}y_j + kA_{1,n+2}\right] \times \frac{1}{ky_1(1 - y_{n+2})}$$

iii) Eq. (11) can be written as follows:

$$(1 - y_{n+2})\sum_{j=2}^{n+1} w_j\Im_{j-1} = \Im_{n+1}\sum_{j=2}^{n+1} w_jy_j \tag{16}$$

The (n + 2) nonlinear equations represented by Eqs. (14)–(16) together with the other two equations as defined by Eqs. (12) and (13) can be written as

functional form as follows:

$$f_i(\underline{y}^{(k+1)}) = y_{i+1}^{(k+1)} - y_{i-1}^{(k)} - \frac{\Delta t}{2}\left[\Im_i^{(k)} + \Im_i^{(k+1)}\right] = 0 \quad \text{for i = 1,2,3, …, n.}$$

$$f_{n+1}(\underline{y}^{(k+1)}) = y_{n+2}{}^{(k+1)} - y_{n+2}{}^{(k)} - \frac{\Delta t}{2}\left[\Im_{n+1}^{(k)} + \Im_{n+1}^{(k+1)}\right] = 0$$

$$f_{n+2}(\underline{y}^{(k+1)}) = \left(1 - y_{n+2}^{(k+1)}\right)\sum_{j=2}^{n+1} w_j \Im_{j-1} - \Im_{n+1}\sum_{j=2}^{n+1} w_j y_j^{(k+1)} = 0$$

$$f_{n+3}(\underline{y}^{(k+1)}) = y_{n+3}^{(k+1)} - \left(\Delta P - \sigma\Delta\pi\right)\left[R_m\mu_s + \alpha y_1 c_b{}'\mu_s \frac{y_{n+2}D}{k(1-y_{n+2})}\right] = 0$$

$$f_{n+4}(\underline{y}^{(k+1)}) = 1 - \frac{y_{n+4}}{y_1} - \frac{\sigma(1-F)}{1-\sigma F} = 0, \text{ where } F = \exp\left[-(1-\sigma)y_{n+3}/P_m\right]$$

(17)

The above set of equations were solved simultaneously by multidimensional Newton–Raphson method from where the increment vector ($\underline{\Delta y}$) can be calculated by solving the following set of equations by Gauss Elimination method.

$$\underline{J}.\underline{\Delta y} = -\underline{f}(\underline{y}) \tag{18}$$

Elements of the Jacobian matrix were evaluated numerically, as suggested by Broyden[22]:

$$\frac{\partial f_i}{\partial y_j} = [f_i(y_1, \ldots, y_{j+h}, \ldots, y_{n+4}) - f_i(y_1, \ldots, y_{j-h}, \ldots, y_{n+4})]/2h \tag{19}$$

where $f_i(y_1, \ldots, y_{n+4}) = 0$ represents i-th equation of the set of (n + 4) number of nonlinear equations. The above equation is written for the evaluation of (n + 4) × (n + 4) order Jacobian matrix. Here, h is a very small quantity and is taken as 0.0001 y_j in most of the cases. Details of the simulation algorithm are shown in Fig. 2. Other methods for the solution of nonlinear equation could have been used. In fact Broyden–Householder method has been applied for eliminating the problem of evaluation of Jacobian matrix in each iteration, but since the original system of equation gives a well convergent set, it produces very little improvement over conventional Newton–Raphson method.

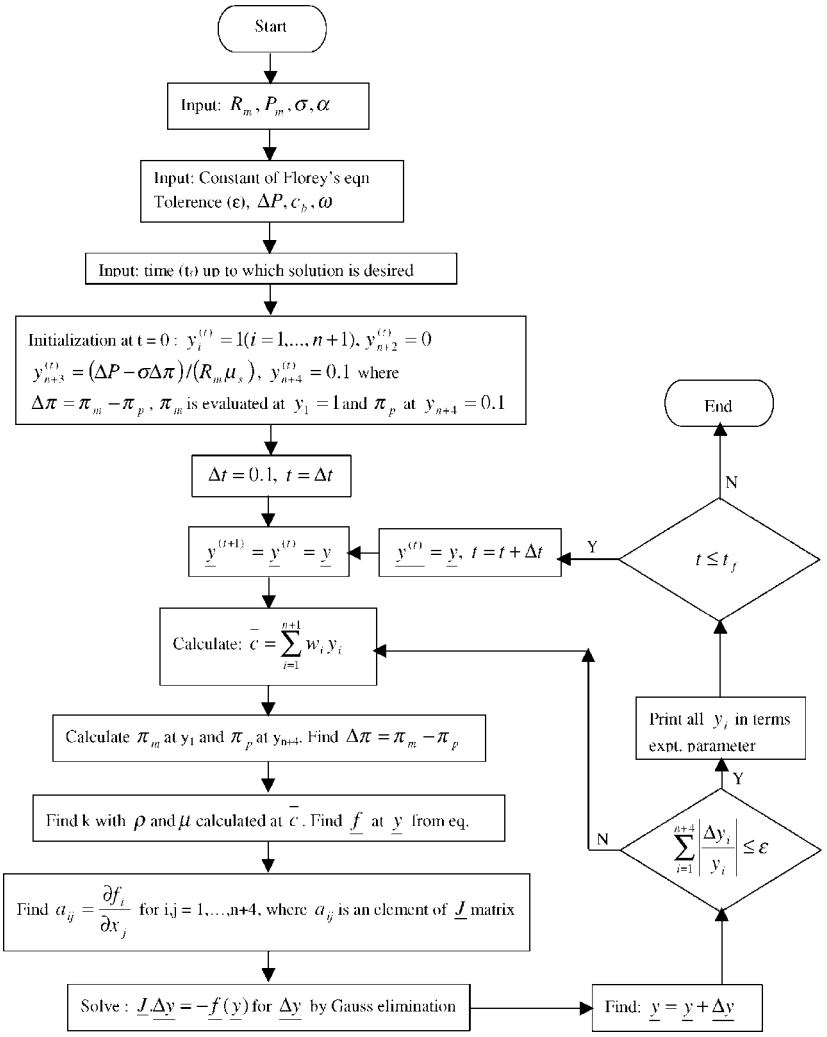

Figure 2. Algorithm for dynamic simulation of flux, rejection, concentration profile, and gel layer thickness.

EXPERIMENTAL

A continuous stirred cell has been used for the purpose of experimentation. Flat disc, asymmetric, hydrophilic cellulose acetate

membrane of MWCO 5000 (obtained from Spectrum Medical Industries, Los Angeles, CA 90060, USA, model: SPECTRA-POR) was used in conjunction with highly porous polymeric support. The diameter of the membrane was 76 mm with effective filtration area $2.64 \times 10^{-3}\,m^2$ and that of stirrer impeller was 56 mm. Solutions of Polyethylene Glycol (PEG-6000) of molecular weight ranging from 6000 to 7500 (obtained from Fluka, England) were prepared using distilled water. The levels of concentration used were 20, 50, and 70 $kg.m^{-3}$, while the pressures were varied as 552, 689, and 827 kPa and the stirrer speed levels were 5.5, 7.5, and 9.0 rps. The concentrations of PEG-6000 in feed and in permeate were measured by refractive index calibration method. The density and viscosity of PEG-6000 solution can be expressed as a function of concentration as follows[16]:

$$\rho = (0.9956 + 0.2776 \times 10^{-3}\, c' - 0.9822 \times 10^{-6} c'^{2}) \times 1000.0 \tag{20}$$

$$\mu = (0.85 + 0.01446c' + 0.02734 \times 10^{-2} c'^{2} - 4.276 \times 10^{-6} c'^{3} + 2.84 \times 10^{-8} c'^{4})/1000.0 \tag{21}$$

Details of the experimental methods, characteristics of membrane, and the ultrafiltration cell were reported elsewhere.[15,16]

RESULTS AND DISCUSSION

For the solution of the above-mentioned set of equations at different time points, some initial guess is necessary. Before that one has to choose a specific value of time increment, Δt. Since an "A–Stable" method has been used here, Δt was assumed to be 0.1 which is expected to give a reasonable accuracy with the implicit method of second order local truncation error (LTE). For evaluating $n + 4$ values of variables at any time, say $t + \Delta t$, all the previous values at time t have been used as initial guess vector. For the first trial, i.e., when evaluating for time $t = \Delta t$, values of all variables at time $t = 0$ were required. For this, all c_i $(i = 1, 2, \ldots, n + 1)$ was chosen as 1.0 (i.e., bulk concentration), z was set to 0.0, J was calculated from the relation $J = (\Delta P - \sigma \Delta \pi)/(R_m \mu_s)$ with $\Delta \pi$ being evaluated based on assumption that bulk concentration prevails over membrane surface and permeate concentration was taken to be 10% of bulk value (i.e., $c_p = 0.1$). With above set of initial guesses, calculation can be started to obtain solution up to any desired time.

Above set of equations were solved for 3-point, 4-point and 5-point OC technique (i.e., $n = 3$, 4, and 5). The results show negligible difference with

increasing number of points in OC. So a 3- or 4-point collocation may be sufficient to yield the results with reasonable accuracy. The mass transfer coefficient appearing in Eqs. (8), (9), (11), and (12) can be evaluated in two ways. The functional dependence of k, as represented by Eq. (6) shows that it is a function of concentration since the viscosity and density may change with concentration. So k can be evaluated at bulk concentration (c_b') or at average concentration prevailing over the effective boundary layer. (Average concentration in dimensionless form is $\bar{c} = \sum_{j=2}^{n+1} w_j c_j$). Results were obtained for the two methods, but the latter shows a closer fit with the experimental data regarding the values of c_p' and J. So k was evaluated based on viscosity and density values evaluated at $\bar{c}$. Since $\bar{c}$ is an unknown quantity, its value has been determined in iteration loop itself.

To start the computations, four parameter values have been first determined from experimental data by using standard procedure as reported by Bhattacharjee and Bhattacharya.[15,16] These values are as follows: $R_m = 1.998 \times 10^{13}\ m^{-1}$, $P_m = 1.8275 \times 10^{-6}\ m\,s^{-1}$, $\alpha = 2.9086 \times 10^{13}\ m\,kg^{-1}$, and $\sigma = 0.98322$. Once the above four parameter values are known, calculation can be started to obtain the concentration profile prevailing in boundary layer, the gel thickness, permeate concentration, and the flux—all as a function of time starting from $t = 0$ to any desired time.

Figure 3 shows the variation of thickness of deposited gel layer along with change in thickness and concentration in "effective" boundary layer. The results are commensurate with the assumption inherent in the model. The total thickness of gel and effective boundary layer remains constant at δ whose value can be obtained from the film theory. The figure shows the result for a specific run under a specific set of operating conditions. At any point within the effective boundary layer, concentration increases with time until the attainment of steady state. Simultaneously, its thickness gets reduced due to the increase of the thickness of deposited "gel" layer. Due to increase of concentration gradient in the effective boundary layer, back diffusive flux increases with the resulting decrease in permeate flux until the attainment of steady state. Permeate flux also decreases due to the increased thickness of deposited solute layer.

Figure 4 shows the variation of steady state concentration profile in the effective boundary layer as a function of pressure differential (Fig. 4a) and stirrer speed (Fig. 4b) keeping all other conditions constant at the prescribed value. Concentration at any point within the effective boundary layer increases with the increase in pressure. Increased driving force increases the permeate flux, which causes more solute molecules to accumulate near the vicinity of the membrane. Due to this reason, concentration at all points increases with pressure differential. Higher stirrer speed causes the reverse effect. Increased

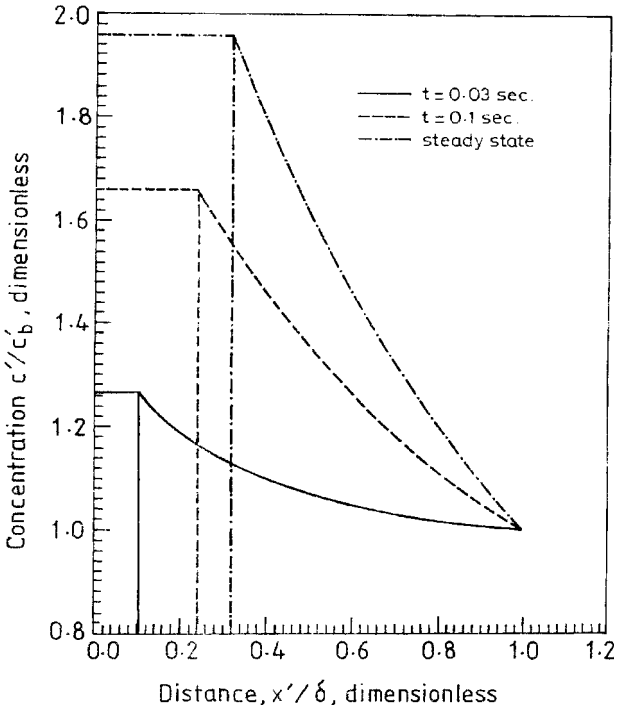

Figure 3. Variation of unsteady state behavior of concentration profile in effective boundary layer and gel thickness vs. dimensionless distance measured from gel surface ($\Delta P = 827\,kPa$, $T = 298\,K$, $c_b' = 20\,kg\,m^{-3}$, $\omega = 9\,rps$).

stirrer speed generates more turbulence in the region adjacent to the membrane surface and this leads to the enhanced rate of transport of the accumulated solutes into the bulk of the solution. This results in the lowering of the concentration with the increase in stirrer speed.

Figure 5 shows the variation of gel thickness as a function of stirrer speed and pressure differential. Increased pressure increases the flux and hence the membrane rejects more solutes. These accumulated solutes increase the gel thickness. With increase in stirrer speed more and more solutes get transported back into bulk and thus the gel thickness decreases. These observations are also in accordance with the result depicted in Fig. 4.

Figure 6 shows the variation of gel thickness and permeate concentration (both in dimensionless forms) as a function of bulk concentration for two runs at different stirrer speeds. The figure shows that with the increase in bulk

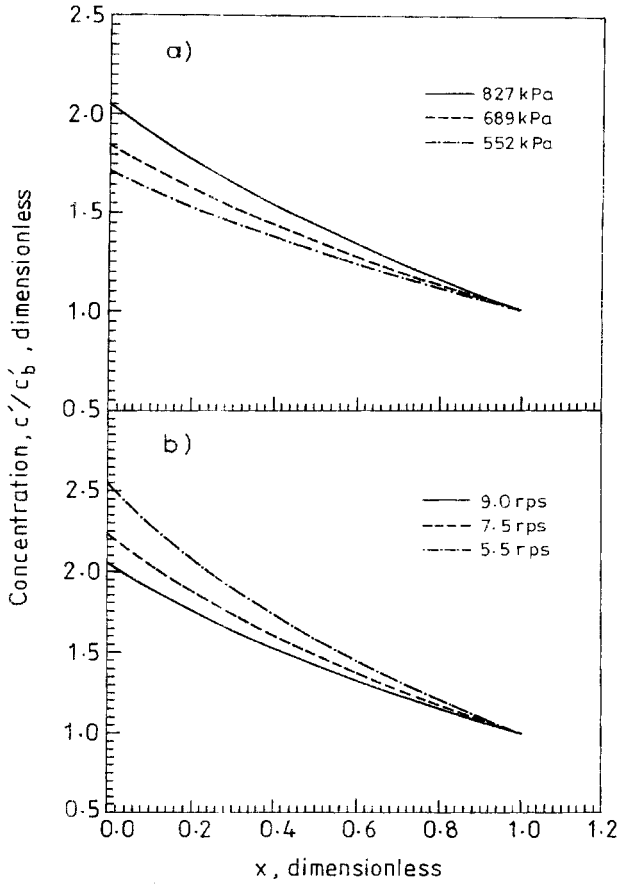

Figure 4. Variation of steady state concentration profile in the effective boundary layer as a function of stirrer speed and pressure differential (a) at constant $c_b' = 20\,\mathrm{kg\,m^{-3}}$, $\omega = 9\,\mathrm{rps}$ and (b) at constant $c_b' = 20\,\mathrm{kg/m^{-3}}$, $\Delta P = 827\,\mathrm{kPa}$ vs. dimensionless distance from gel surface (T = 298 K).

concentration, the ratio c_p'/c_b' should increase and this means that rejection should decrease. Increased bulk concentration increases the concentration driving force across the membrane, which may cause more solute molecules to diffuse through the pores of the membrane. This may be the reason for the decrease of rejection with the increase in bulk concentration.

Figure 7 shows the dependence of c_p'/c_b' ratio on the values of stirrer speed and pressure differential. Increased pressure differential increases the flux, causing

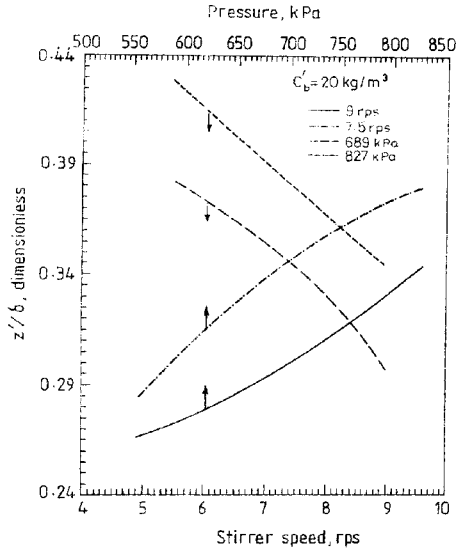

Figure 5. Variation of gel (or, cake) thickness as a function of stirrer speed and pressure differential ($c_b' = 20\,\text{kg.m}^{-3}$ and $T = 298\,\text{K}$).

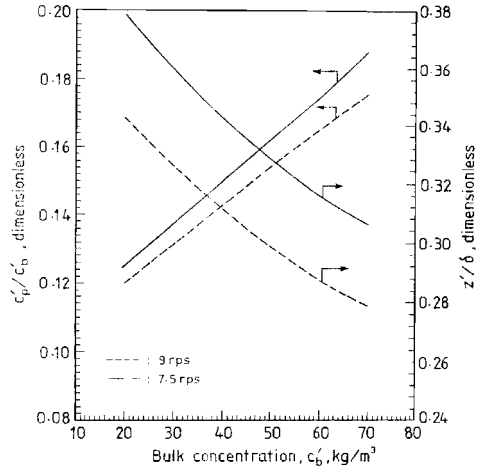

Figure 6. Variation of gel thickness and permeate concentration (in dimensionless form) as a function of bulk concentration ($\Delta P = 827\,\text{kPa}$, $T = 298\,\text{K}$).

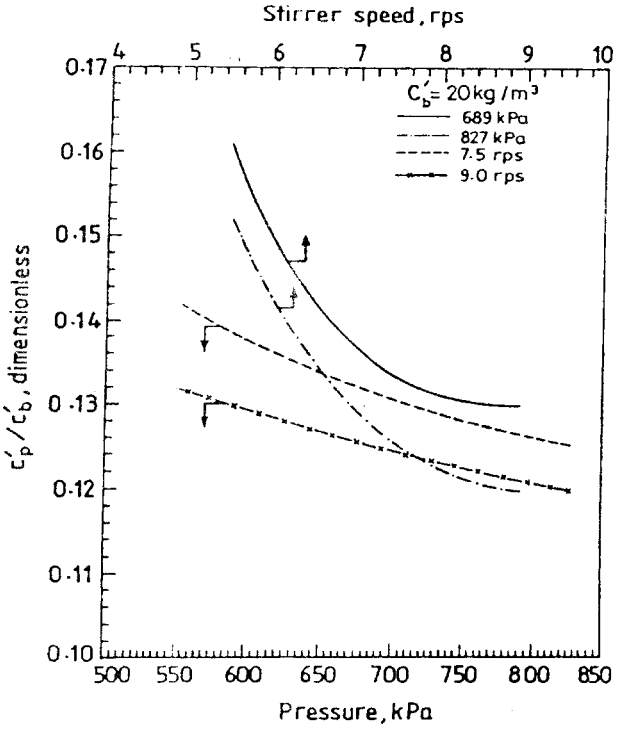

Figure 7. Variation of permeate concentration (in dimensionless form) as a function of stirrer speed and pressure differential ($c_b' = 20\,\mathrm{kg\,m^{-3}}$ and T = 298 K).

more solute deposition, which implies higher thickness of deposited solute or "gel" layer. This deposited solute layer acts as a secondary membrane and with its extra sieving action, it causes more solutes to be retained. The above effect not only reduces the permeate concentration but also increases the rejection. Increased pressure also has the effect of compressing the deposited layer to enable it to act more like a compact membrane. It ultimately reduces the permeability of the solute molecules. Higher stirrer speed reduces the gel thickness due to increased rate of turbulent transport of deposited solute into bulk. This decrease in thickness of the deposited layer causes the effect of "secondary membrane" to decrease, thus reducing the extra sieving action achieved by the deposited gel layer. Due to this reason, permeate concentration decreases with the increase in stirrer speed.

The permeate concentration and flux calculated by this model agree well with the experimental data. Comparisons of predicted flux and experimental

flux have been shown in Figs. 8, 9, and 10, which are showing the simulated flux data in comparison with experimental flux data under varying pressure difference, bulk concentration, and stirrer speed respectively. Figure 8 shows that with the increase in pressure, flux should increase, if all other conditions remain constant. Increase of pressure causes more driving force, hence the flux should increase. The decrease of flux with increase in bulk concentration is manifested in Fig. 9. Increased bulk concentration means more solute deposition on the membrane surface, higher membrane surface concentration, larger effect of concentration polarization, and greater gel thickness. These will cause the flux to decline with increasing bulk concentration. Figure 10 shows the effect of change of stirrer speed on permeate flux. With increase in stirrer speed, the flux increases because of higher turbulence, lesser gel effect, and finally, the reduced effect of concentration polarization. These three figures show that deviations in the simulated flux are quite low in comparison to experimental results. Figure 11 shows the comparison of the predicted rejections values with experimental data. This figure also shows that in most

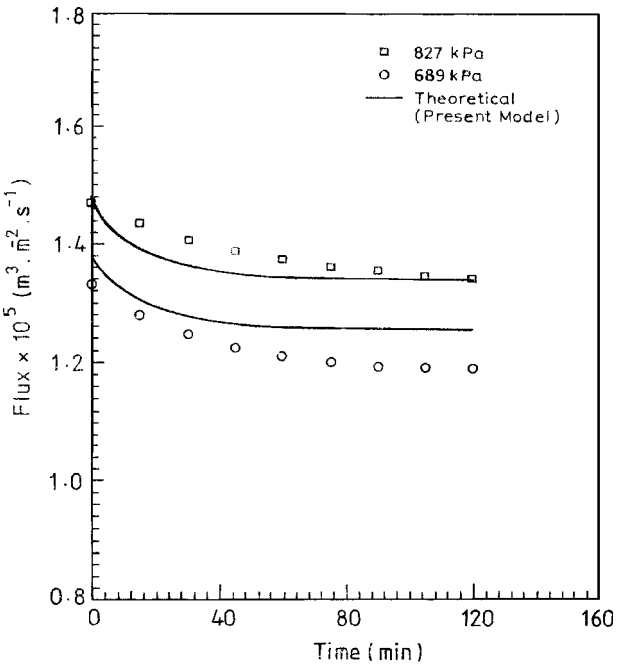

Figure 8. Variation of simulated and experimental permeate flux as a function of transmembrane pressure vs. time ($c_b' = 50\,\mathrm{kg\,m^{-3}}$, $\omega = 5.5$ rps, T = 298 K).

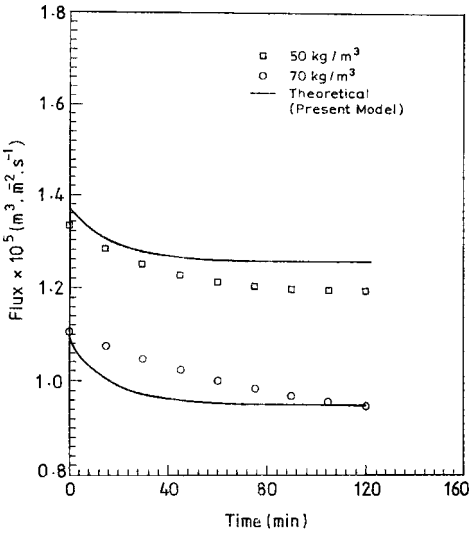

Figure 9. Variation of simulated and experimental permeate flux as a function of bulk concentration vs. time ($\omega = 5.5$ rps, $\Delta P = 689$ kPa, $T = 298$ K).

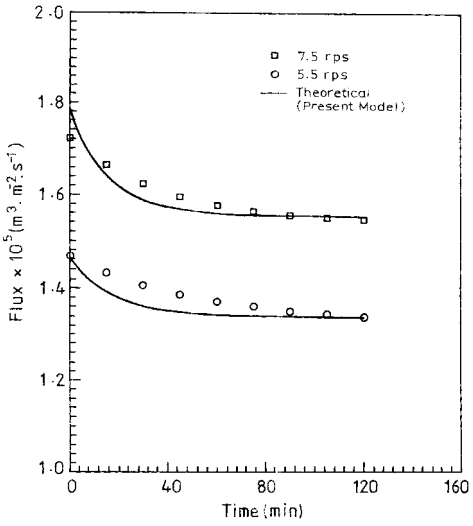

Figure 10. Variation of simulated and experimental permeate flux as a function of stirrer speed vs. time ($c_b' = 50\,\text{kg.m}^{-3}$, $\Delta P = 827$ kPa, $T = 298$ K).

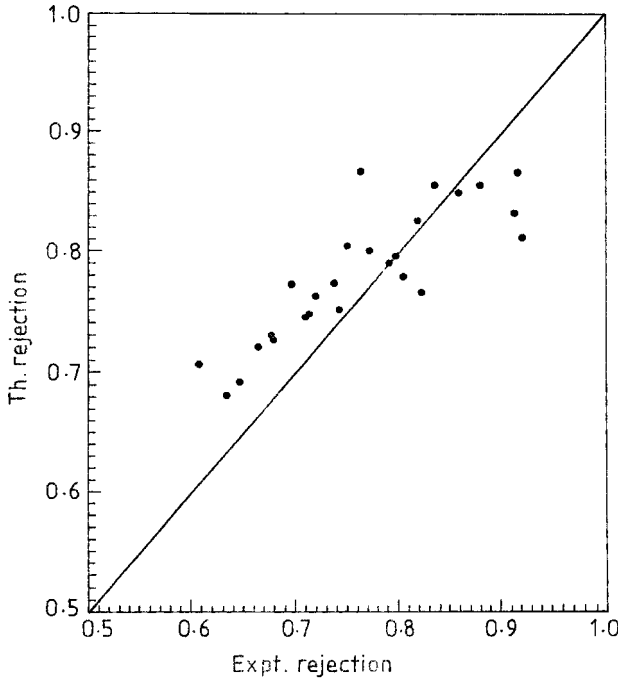

Figure 11. Comparison of the experimental and theoretical rejection predicted from the present model.

cases, the deviation remains within ±10%. The final values of all the variables and their variations with different process parameters are found to be in accordance with the general notions and expectations. So the model seems to give good results as regard to prediction of flux and rejection and analysis of transport phenomena, particularly in the vicinity of the membrane.

CONCLUSIONS

A mass transfer model for the simulation of ultrafiltration process has been developed in this study which is capable of analysis of boundary layer phenomena together with gel formation and prediction of permeate flux and rejection at a specified operating condition. The variation of concentration gradient in the effective boundary layer and the thickness of gel layer have also been studied under different operating conditions. The combined effect

due to increase in concentration gradient and increase in gel layer thickness on permeate flux has been established under dynamic conditions as well as in the steady state. The predicted results from the model show good agreement with experimental data and are consistent with the assumptions inherent in the model and general notions regarding separation of macro molecular solutes by ultrafiltration. The calculation procedure reported here is for dead-end ultrafiltration. Nevertheless, the simulation procedure is also valid for cross-flow filtration. The only difference will be in the calculation of the mass transfer coefficient, and thereby the corresponding thickness of the gel layer and effective concentration boundary layer (δ). In this study, it has been proposed that this thickness (δ) remains constant during the UF process. In dead-end ultrafiltration, this overall thickness is limited by the stirring action created by the stirrer, whereas in cross-flow ultrafiltration, it is limited by the turbulence created by the flowing fluid, due to which concentration boundary layer cannot extend indefinitely from the membrane surface.

NOMENCLATURE

Symbols

$\mathbf{A}$	collocation matrix
A_{ij}	element in i-th row and j-th column of $\mathbf{A}$ matrix
$\mathbf{B}$	collocation matrix; B_{ij} an element in that matrix
c'	concentration ($kg\,m^{-3}$); c'_b—bulk concentration, c'_p—permeate conc., c'_m—membrane surface conc.
c	dimensionless concentration $= c'/c'_b$, c_i—at i-th collocation point; c_b, c_p, c_m means bulk, permeate, and membrane surface conc., respectively.
D	diffusivity ($m^2\,s^{-1}$)
$\Im_i$	function defined by equation (14) and (15)
f_i	ith nonlinear function defined by Eq. (17), for $i = 1, 2, \ldots, n+4$
$\underline{f}$	function vector containing all the functions as defined by Eq. (17)
F	a dimensionless constant, defined in Eq. (13)
h	increment in independent variable (defined in Eq. 19)
J	permeate flux ($m^3\,m^{-2}\,s^{-1}$), J_o—permeate flux at time zero
$\underline{J}$	Jacobian matrix of order $(n+4) \times (n+4)$, (Eq. 18)
k	mass transfer coefficient ($m\,s^{-1}$)

M	molecular weight ($kg\,kmol^{-1}$)
P	pressure (Pa)
P_m	solute permeability ($m\,s^{-1}$)
r	radius of the membrane (m)
R_m	membrane hydraulic resistance (m^{-1})
t'	time (s)
t	dimensionless time $= Dt'/\delta^2$
w_i	weightage factor for the i-th collocation point
x'	distance from the membrane (m)
x	dimensionless distance measured from gel surface, defined in Eq. (3), x_i—distance of the i-th point
y	unknown variables (dimensionless), $y_1, y_2, \ldots, y_{n+4}$
$\underline{y}$	unknown column vector containing all the elements $y_1, y_2, \ldots, y_{n+4}$
z'	gel thickness (m)
z	dimensionless thickness $= z'/\delta$

Abbreviations

MWCO	molecular weight cut off
OC	orthogonal collocation
PEG	poly ethylene glycol
UF	ultrafiltration

Greek Letters

α	specific cake resistance ($m\,kg^{-1}$)
δ	total thickness of gel and concentration boundary layer (m)
μ	viscosity (Pa s)
ρ	density ($kg\,m^{-3}$)
π	osmotic pressure (Pa)
ω	angular velocity (s^{-1})

REFERENCES

1. Aimar, P.; Field, R. Limiting flux in membrane separation: a model based on the viscosity dependency of mass transfer coefficient. Chem. Eng. Sci. **1992**, *47*, 579.
2. Field, R.; Aimar, P. Ideal limiting flux in ultrafiltration: comparison of various theoretical relationships. J. Membr. Sci. **1993**, *80*, 107.

3. Blatt, W.F.; Dravid, A.; Michael, A.S.; Nelsen, L. Solute polarization and cake formation in membrane ultrafiltration: causes, consequences and control techniques. In *Membrane Science and Technology*; Flinn, J.E., Ed.; Plenum Press: New York, 1970; 47–97.
4. Wijmans, J.G.; Nakao, S.; Smolders, C.A. Flux limitation in ultrafiltration: osmotic pressure model and gel layer model. J. Membr. Sci. **1984**, *20*, 115.
5. Danes, F.E.; Boriou, B.; Poyen, S. Effects of diffusion and osmosis on flux decline during ultrafiltration with total rejection on an unstirred batch cell. J. Membr. Sci. **1990**, *50*, 177.
6. Nakao, S.; Yumoto, S.; Kimura, S. Analysis of rejection characteristics of macromolecular gel layer for low molecular weight solutes in ultrafiltration. J. Chem. Eng. Jpn. **1982**, *15* (6), 463.
7. Lebrun, R.E.; Bouchard, C.R.; Rollin, A.L.; Matsura, T.; Sourirajan, S. Computer simulation of membrane separation processes. Chem. Eng. Sci. **1989**, *44* (2), 313.
8. Song, L.; Elimelech, M. Theory of concentration polarization in cross flow filtration. J. Chem. Soc. Faraday Trans. **1995**, *91* (19), 3389.
9. Youm, K.H.; Fane, A.G.; Wiley, D.E. Effects of natural convection instability on membrane performance in dead end and cross flow ultrafiltration. J. Membr. Sci. **1996**, *116*, 229.
10. Redkar, S.; Kuberkar, V.; Davis, R.H. Modeling of concentration polarization and depolarization with high frequency back pulsing. J. Membr. Sci. **1996**, *121*, 229.
11. Bhattacharjee, S.; Sharma, A.; Bhattacharya, P.K. A unified model for the flux prediction during batch cell ultrafiltration. J. Membr. Sci. **1996**, *111*, 243.
12. de Pinho, N.N.; Semiao, V.; Geraldes, V. Integrated modeling of transport processes fluid/nanofiltration membrane system. J. Membr. Sci. **2002**, *206* (1–2), 189.
13. Paris, J.; Guichardon, P.; Charbit, F. Transport phenomena in ultrafiltration: a new two-dimensional model compared with classical models. J. Membr. Sci. **2002**, *207* (1), 43.
14. Bhattacharjee, C.; Bhattacharya, P.K. Prediction of limiting flux in ultrafiltration of kraft black liquor. J. Membr. Sci. **1992**, *72*, 137.
15. Bhattacharjee, C.; Bhattacharya, P.K. Flux decline analysis in ultrafiltration of kraft black liquor. J. Membr. Sci. **1993**, *82*, 1.
16. Neimi, H.; Raimoaho, J.; Palosaari, S. Modeling and simulation of ultrafiltration and reverse osmosis process. Acta Polytech. Scand. Chem. Technol. Metall. Ser. No. 174, Helsinki **1986**.

17. Nguyen, Q.T.; Aptel, P.; Neel, J. Characterization of ultrafiltration membranes, Part II. Mass transport measurements for low and high molecular weight synthetic polymer in water solution. J. Membr. Sci. **1980**, *7*, 141.
18. Sherwood, T.K.; Pigford, R.L.; Wilke, C.R. *Mass Transfer*; McGraw Hill: NewYork, 1975.
19. Finlayson, B.A. *Nonlinear Analysis in Chemical Engineering*; McGraw Hill: NewYork, 1980.
20. Flory, P.J. *Principles of Polymer Chemistry*; Cornell University Press: Ithaca, NY, 1953.
21. Nakao, S.; Kimura, S. Analysis of solute rejection in ultrafiltration. J. Chem. Eng. Jpn. **1981**, *14*, 32.
22. Broyden, C.G. A class of methods for solving nonlinear simultaneous equations. Math. Comput. **1965**, *19*, 577.

Received January 2002
Revised October 2002